Nanoscale

PAPER

View Article Online
View Journal | View Issue

Cite this: *Nanoscale*, 2022, **14**, 17297

Graphene oxide modulates dendritic cell ability to promote T cell activation and cytokine production†

Helen Parker, [a] Alfredo Maria Gravagnuolo, [b,c] Sandra Vranic, [b,c] Livia Elena Crica, [b,c] Leon Newman, [b,c] Oliver Carnell, [a] Cyrill Bussy, [a,b,c] Rebecca S. Dookie, [a] Eric Prestat, [d,e] Sarah J. Haigh, [c,d] Neus Lozano, [f] Kostas Kostarelos [b,c,f] and Andrew S. MacDonald *[a]

An important aspect of immunotherapy is the ability of dendritic cells (DCs) to prime T cell immunity, an approach that has yielded promising results in some early phase clinical trials. However, novel approaches are required to improve DC therapeutic efficacy by enhancing their uptake of, and activation by, disease relevant antigens. The carbon nano-material graphene oxide (GO) may provide a unique way to deliver antigen to innate immune cells and modify their ability to initiate effective adaptive immune responses. We have assessed whether GO of various lateral sizes affects DC activation and function *in vitro* and *in vivo*, including their ability to take up, process and present the well-defined model antigen ovalbumin (OVA). We have found that GO flakes are internalised by DCs, while having minimal effect on their viability, activation phenotype or cytokine production. Although adsorption of OVA protein to either small or large GO flakes promoted its uptake into DCs, large GO interfered with OVA processing. In terms of modulation of DC function, delivery of OVA *via* small GO flakes significantly enhanced DC ability to induce proliferation of OVA-specific $CD4^+$ T cells, promoting granzyme B secretion *in vitro*. On the other hand, delivery of OVA *via* large GO flakes augmented DC ability to induce proliferation of OVA-specific $CD8^+$ T cells, and their production of IFN-γ and granzyme B. Together, these data demonstrate the capacity of GO of different lateral dimensions to act as a promising delivery platform for DC modulation of distinct facets of the adaptive immune response, information that could be exploited for future development of targeted immunotherapies.

Received 20th April 2022,
Accepted 24th October 2022

DOI: 10.1039/d2nr02169b

rsc.li/nanoscale

Dendritic cells (DCs) are important innate antigen (Ag) presenting cells (APCs) that patrol tissues for foreign organisms and materials, which they have potent ability to recognise, capture and process for presentation to, and activation of, T cells.[1,2] The composition of such Ags, and environmental signals present during their uptake, directly impacts DC activation and function, conferring immunogenic or tolerogenic ability.[3–6] Pathogens, microbial or danger associated molecular patterns (PAMPs, MAMPs or DAMPs), and Ags containing or contaminated with such (including endotoxins), can enable DCs to promote the activation and differentiation of T cells into diverse effector states (T_{eff}).[7] These cues usually trigger DC activation, termed 'maturation', whereby Ag processing is enhanced, expression of peptide major histocompatibility complexes (MHCII/MHCI) and co-stimulatory molecules is increased, and cytokines necessary for T_{eff} polarisation are produced.[8] DCs also possess the ability to induce tolerance to innocuous signals,[9] in part by promoting the differentiation of naïve T cells into immunosuppressive regulatory T cells (T_{regs}). Thus, how DCs encounter and respond to Ag plays a pivotal role in shaping their capacity to modify the character of T cell responses.[5,10]

The central ability of DCs to induce and direct Ag specific T cell responses has highlighted the potential effectiveness of these specialised immune cells in immunotherapy of cancer, autoimmune diseases and transplant rejection.[11–14] DC based immunotherapy has yielded promising results in early phase

[a]*The Lydia Becker Institute of Immunology and Inflammation, University of Manchester, UK. E-mail: andrew.macdonald@manchester.ac.uk*
[b]*Nanomedicine Lab, University of Manchester, UK. E-mail: kostas.kostarelos@manchester.ac.uk*
[c]*National Graphene Institute, University of Manchester, UK*
[d]*School of Materials, University of Manchester, UK*
[e]*SuperSTEM Laboratory, SciTech Daresbury Campus, Daresbury, WA4 4AD, UK*
[f]*Catalan Institute of Nanoscience and Nanotechnology (ICN2), CSIC and BIST, Campus UAB, Bellaterra, 08193 Barcelona, Spain*
† Electronic supplementary information (ESI) available. See DOI: https://doi.org/10.1039/d2nr02169b

clinical trials for conditions such as breast cancer, rheumatoid arthritis, multiple sclerosis and solid organ rejection after transplant.[15–18] However, candidate Ags can be poorly immunogenic, and the efficacy of methods employed to boost protective responses, such as adjuvants, can be variable.[19,20] Therefore, more refined approaches are needed to enhance DC ability to generate appropriate immune responses against candidate therapeutic Ags.

A variety of nanomaterials are finding applications in the therapy of cancer. Functionalised carbon nanoparticles can be used as molecular carriers for drug delivery, due to their ability to enhance cellular uptake of Ags.[21,22] More recently, graphene has also attracted increasing interest with regards to its biomedical applications. Graphene has a variety of physiochemical characteristics relevant to biomedical application, including a very large surface area and high mechanical strength and flexibility, that play a critical role in determining their interactions with biological matter.[23,24] Graphene oxide (GO), an oxidised derivative of graphene, is rich in oxygen groups that significantly increase its hydrophilicity and biocompatibility, while its large surface area and functional groups allow for efficient conjugation and loading of bioactive molecules.[25] This high loading capacity has started to be exploited for the delivery of anti-cancer genes, tumour Ags and chemotherapeutics.[26] However, limited information is available regarding the inherent immunogenicity of GO, as well as its impact on the ability of DCs to initiate and direct immune responses.

Although various carbon nanoparticles, including GO, are readily taken up by DCs,[27] current evidence on how GO influences DC activation and function is somewhat conflicting.[28,29] One recent study demonstrated that GO loaded with the glioma Ag survivin induces a potent DC-mediated anti-glioma response *in vitro*.[30] However, an earlier study suggested that GO inhibits DC presentation of the model Ag OVA, dependent on down regulation of the immunoproteasome Ag processing subunit LMP7, responsible for MHCI presentation.[27] Further, GO lateral dimensions may be a crucial factor in material uptake and innate cell activation, with large GO (LGO) able to promote more pro-inflammatory polarisation in a murine macrophage cell line, as well as in *in vivo* murine models.[31] In contrast, small GO (sGO) flakes appear to elicit activation of human monocytes, when compared to large.[32] It is becoming increasingly clear that it is vital to understand whether conflicting reports of GO inflammatory potential are a result of material production method variability, including possible levels of endotoxin contamination.[33]

We have carefully investigated the immunogenicity of endotoxin-free GO of different lateral dimensions and defined its impact on DC activation and function *in vitro* and *in vivo*, including ability to take up, process and present OVA to $CD4^+$ and $CD8^+$ T cells. We found that sGO flakes were readily internalised by DCs, while having minimal effect on their viability, activation phenotype or cytokine production. LGO flakes were found to predominantly interact with the plasma membrane of DCs, while displaying a similarly muted impact on DC viability or activation. Although adsorption of OVA protein to either small or LGO flakes promoted its uptake into DCs, LGO interfered with its processing. In terms of modulation of DC function, delivery of OVA *via* sGO flakes significantly enhanced DC ability to induce proliferation of OVA-specific $CD4^+$ T cells *in vitro*. On the other hand, delivery of OVA *via* LGO flakes augmented DC ability to induce proliferation of OVA-specific $CD8^+$ T cells, and their production of IFN-γ and granzyme B. These data establish that endotoxin-free GO of different lateral dimensions displays minimal inherent ability to induce DC maturation. Despite this, they also show that GO flake lateral dimension governs DC ability to promote Ag-specific $CD4^+$ or $CD8^+$ T cell activation, proliferation and cytokine secretion. This information increases fundamental understanding of the biological effects of GO derivatives on immune response induction, which could enable future development of novel immunotherapies for diverse conditions in which the modulation of cellular immunity is critical.

Results

Synthesis and characterisation of small and large GO flakes

In order to synthesise thin (one to two layers thickness), highly pure and endotoxin-free GO of different lateral dimensions for biomedical applications, we have optimised the modified Hummers' method.[34] Exhaustive characterisation of sGO and LGO was performed as previously described[34] and is summarised in Table S1 and Fig. S1, S2.† Aqueous suspensions of GO were well-dispersed, brownish in colour, stable at room temperature, and of no endotoxin content (using a TNF-α expression assay) (Table S1 and Fig. S1†).

GO affects DC viability in lateral size and dose dependent manner

To explore the potential of GO as an immunomodulator for targeting of DCs in biomedical applications, as well as a potential platform for DC mediated immunotherapies, we assessed the effect of LGO and sGO on DCs in culture, initially focussing on viability. Variable concentrations of LGO and sGO were incubated with murine bone marrow derived DCs (BMDCs) for 18 h, and their viability assessed by flow cytometry. LGO or sGO at lower concentrations exhibited negligible toxicity against DCs (Fig. 1A), with significantly reduced viability only evident at the higher doses of LGO, and the highest dose of sGO (Fig. 1A and B). Based on these data, 5 μg ml^{-1} sGO or LGO was employed in subsequent experiments.

Internalisation of sGO and LGO by DCs

To identify how effectively GO flakes were internalized, BMDCs were cultured with 5 μg ml^{-1} sGO or LGO for 18 h. An overlay of confocal DIC images with Raman spectroscopy 2D mapping showed definitive co-localisation of the typical GO Raman shift with BMDCs (Fig. 1C). However, it was not possible to conclude definitively from these images whether GO was located intracellularly or attached to the surface membrane of the

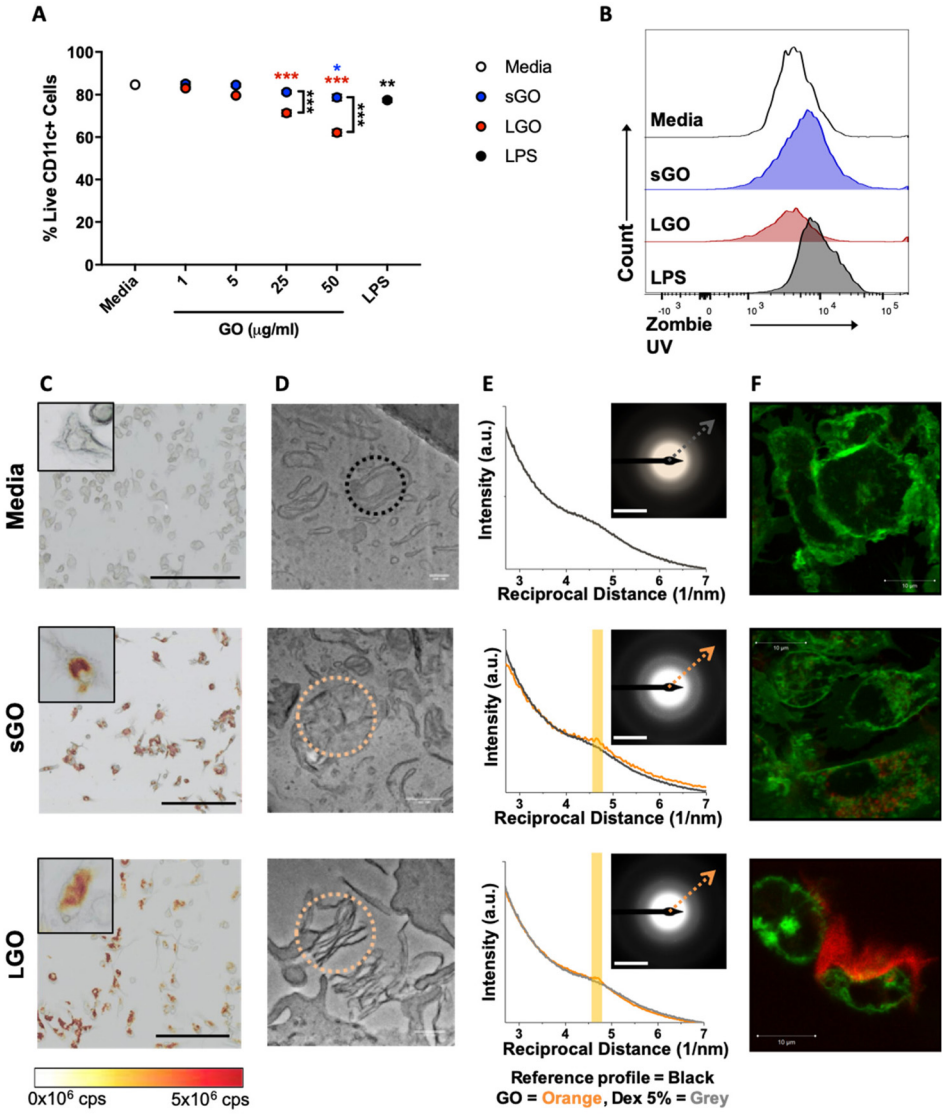

Fig. 1 Effects of GO lateral size on bone marrow derived dendritic cell viability and internalisation pattern. (A and B) BMDCs were incubated with sGO or LGO at a range of concentrations or LPS (100 ng ml^{-1}) for 18 h. (A) Cellular viability was assessed *via* Zombie UV dye exclusion in CD11c^{+} DCs. (B) A representative flow cytometry histogram demonstrating Zombie UV negative DCs after 50 μg ml^{-1} GO. (C–F) BMDCs were incubated with media, sGO (5 μg ml^{-1}) or LGO (5 μg ml^{-1}) for 18 h and GO localisation was assessed. (C) Raman mapping allowed for localisation of GO relative to DCs following GO challenge. Raman mapping (λ = 633 nm, 0.4 mW, area size = 0.3 mm^2, spatial resolution = 1 μm) of DCs challenged with media only (control), sGO or LGO. Representative images are provided for each condition (insets provide higher magnification for each sample). GO abundance is measured in counts per second (cps) of Raman scattered photons per second (n = 9). Scale bar: 200 μm. (D) Representative ultra-structural interactions of dendritic cells with sGO and LGO shown using TEM, at high magnification (scale bar: 200 nm for control, 500 nm for sGO and LGO). (E) Representative selected area electron diffraction (SAED) pattern of each sample were obtained in respective regions circled in (D) to evidence the crystalline nature of the material probed, hence confirming presence or absence of GO (small peak in orange profile). For clarity, the profiles of the SAED patterns are given relative to the reference resin SAED profile, here in black. The region of the reciprocal distance of 4.7 nm^{-1} has been highlighted in yellow. At this reciprocal distance, from the centre of the SAED pattern, the lattice reflection of graphene [10, 10] innate to this carbon crystal is expected to result in a peak, as can be observed in both sGO and LGO treated samples. (F) Uptake of GO (excitation at 594 nm/emission at 620–690 nm, red) was imaged using a confocal microscope. DC plasma membranes were stained with CellMask Green plasma membrane stain (excitation at 488 nm/emission max at 520 nm, green). Scale bars represent 10 μm. (A) The data are shown as mean ± STDEV (data is representative of 1 of 3 independent experiments each with 3 intra experimental replicates). Data were analysed using two-way ANOVA with Bonferroni's *post hoc* test, *p < 0.05 **p < 0.01 ***p < 0.001. (B) * above symbols *versus* control.

cells. Transmission electron microscopy (TEM) was therefore performed on cell sections and showed that sGO was clearly located in intracellular regions of the BMDCs, whilst LGO was aligned with the plasma membrane (Fig. 1D). In these TEM images, the nature of the materials found in cells (sGO) or their close vicinity (LGO) was confirmed using Selected Area Electron Diffraction (SAED), which highlighted the typical electron diffraction of graphene crystals absent in non exposed

cells (Fig. 1E). Consistent with the TEM images (Fig. 1D), live cell confocal microscopy exploiting the autofluorescent properties of GO showed that sGO was readily taken up by BMDCs and localised to an intracellular vesicular compartment, whereas LGO was more associated with the extracellular plasma membrane (Fig. 1F).

GO has minimal impact on DC activation

DCs can express a wide range of surface proteins that reflect their activation phenotype and function.[35] Immature BMDCs were cultured for 18 h with sGO (5 μg ml^{-1}), LGO (5 μg ml^{-1}), medium alone as a negative control or LPS (100 ng ml^{-1}) as a positive control and expression of maturation markers CD86, CD80, CD40, CD83, MHCII and MHCI were evaluated by flow cytometry. sGO or LGO had little effect on expression of CD86, CD80, CD40 or MHCII, when compared to medium alone (Fig. 2A, B and Fig. S3†). However, both sGO and LGO significantly increased expression of the putative costimulatory molecule CD83 (Fig. 2A, B and Fig. S3†).[36] LGO also caused a small, but significant, increase in the expression of MHCI and MHCII (Fig. 2B and Fig. S3†). Similar to maturation marker expression, GO had little measurable effect on DC cytokine secretion. sGO failed to stimulate production of the inflammatory mediators TNF-α, IL-6, IL-12p40, IL-12p70, or regulatory IL-10, when compared to medium alone (Fig. 2C). In contrast, LGO induced a small but significant increase in DC production of TNF-α, IL-6 and nitric oxide (NO) (Fig. 2C). Together, these data indicate that neither sGO nor LGO dramatically activate BMDCs in terms of surface phenotype or cytokine production.

GO modifies DC Ag uptake and processing

A key function of DCs is the Ag-specific activation of T cells, a process that relies on efficient protein uptake, intracellular processing and presentation of antigenic peptides *via* MHC/peptide complexes to T cells *via* their surface receptors (TCRs).[35,37] To determine how GO might alter Ag-presenting activity of DCs, we first assessed whether GO could affect initial uptake of OVA. Taking advantage of the physicochemical properties of GO, which allow for efficient loading of bioactive proteins, we adsorbed OVA conjugated to the pH insensitive fluorophore AlexaFluor 647 to sGO or LGO. BMDCs were incubated with OVA_{AF647} or GO–OVA_{AF647} complexes, and uptake of fluorescent OVA assessed by flow cytometry (Fig. 3A). Approximately 2–3 times more DCs internalised Ag when bound to sGO or LGO than soluble OVA alone (Fig. 3B and C). Live cell confocal microscopy showed that OVA_{AF647} localised to an intracellular compartment when DCs were incubated with OVA_{AF647} alone or sGO–OVA_{AF647} complexes (Fig. 3D). However, less uptake was observed upon treatment with LGO–OVA_{AF647} (Fig. 3D), which correlated with the histogram in Fig. 3B highlighting fluorescence on a per cell basis. Next, we investigated the effect of GO on OVA processing using a pH-insensitive self-quenching OVA conjugate (OVA_{DQ}), which fluoresces upon lysosomal proteolysis (Fig. 3E). OVA_{DQ} was adsorbed to sGO or LGO, then DCs incubated with OVA_{DQ} or GO–OVA_{DQ} complexes, and degradation of OVA assessed by flow cytometry. DC uptake of OVA_{DQ} alone resulted in its degradation, as expected (Fig. 3F), with adsorption of OVA_{DQ} to sGO having no measurable effect on this. However, adsorption to LGO significantly attenuated OVA degradation when compared to OVA_{DQ} alone (Fig. 3F). Processing of OVA_{DQ} was assessed by live cell confocal microscopy, which corroborated the uptake and processing kinetics determined by flow cytometry (Videos S1–S4†). Together, these results reveal that size is an important factor in determining GO influence over DC internalisation and/or degradation of protein Ags.

GO Ag delivery modifies DC activation of $CD4^+$ T cells

To determine the influence of GO on DC ability to provide surface MHC-restricted Ag and costimulation for T cell activation, OVA alone, or OVA adsorbed to sGO or LGO (Fig. S2†), was added to immature BMDCs, which were then co-cultured with CFSE-labelled OT-II $CD4^+$ T cells (Fig. 4A). T cell proliferation was then assessed by flow cytometry (Fig. 4B and C). Although co-culture with naïve DCs or DCs pulsed with soluble OVA protein induced limited T cell proliferation, OVA adsorbed to sGO or LGO resulted in comparatively more T cell division (Fig. 4B and C). Notably, sGO–OVA DCs induced significantly more $CD4^+$ T cell proliferation than LGO–OVA DCs (Fig. 4B and C). In contrast to the enhanced DC induction of $CD4^+$ T cell proliferation evident with GO adsorbed to OVA protein, GO adsorbed to MHCII-restricted OVA peptide (OVA_{323}; $OVA_{323–339}$; ISQAVHAAHAEINEAGR) interfered with DC induction of OT-II proliferation (Fig. 4D and E).

In terms of cytokines, the level of IL-2, responsible for proliferation and differentiation of $CD4^+$ T cells into effector T cells (T_{eff}), regulatory T cells (T_{reg}) and memory T cells,[38] was significantly upregulated in DC/OT-II co-cultures containing sGO–OVA DCs, compared to DCs exposed to OVA alone or LGO–OVA (Fig. 5A). Th1 associated IFN-γ, Th2 associated IL-4, IL-5 and IL-13, Th17 associated IL-17A or T_{reg} associated IL-10 were all undetectable, regardless of culture conditions. However, the level of secreted granzyme B, a cytotoxic protease typically released by $CD8^+$ T cells,[39] was also found to be significantly increased in co-cultured OT-II cells with sGO–OVA or LGO–OVA treated DCs (Fig. 5A). In addition to modulating OVA-specific proliferation and cytokine secretion, GO when adsorbed to OVA significantly increased DC induction of the IL-2 receptor alpha chain CD25 on OT-II cells, and increased expression of Foxp3 on dividing OT-II cells (Fig. S4A and B†). In keeping with impaired proliferation (Fig. 4D and E), OT-II cells cultured with sGO–OVA_{323} or LGO–OVA_{323} DCs showed reduced cytokine production in comparison to those cultured with OVA_{323}DCs (Fig. 5B).

Together, these data indicate that GO, and sGO in particular, can enhance the ability of DCs to process and/or present protein Ag to activate $CD4^+$ T cells. In notable contrast, they also suggest that either sGO or LGO impair DC ability to present exogenous peptides to $CD4^+$ T cells.

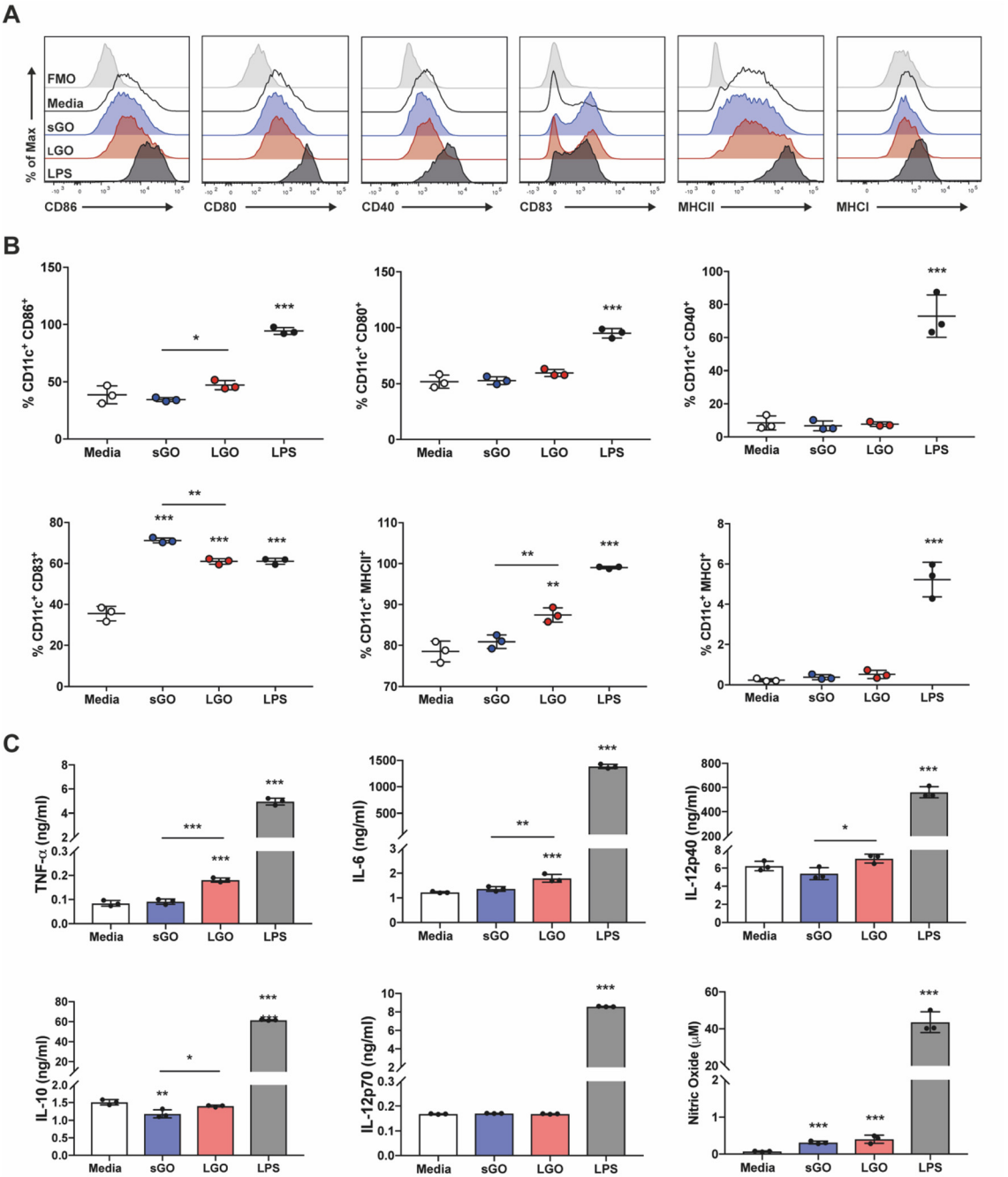

Fig. 2 Graphene oxide has minimal effect on BMDC activation and cytokine production. BMDCs were incubated with medium alone, sGO (5 μg ml^{-1}), LGO (5 μg ml^{-1}) or LPS (100 ng ml^{-1}) for 18 h and (A) phenotypic activation analysed by flow cytometry. (B) % of $CD11c^+$ cells expressing CD86, CD80, CD40, CD83, MHCII and MHCI, as assessed by flow cytometry (C) Levels of cytokines TNF-α, IL-6, IL-12p40, IL-10, IL-12p70, and nitric oxide (NO), secreted into the media, as analysed by ELISA. Data are presented as mean ± STDEV (data is representative of 1 of 3 independent experiments each with 3 intra experimental replicates). Statistical analysis was performed by one-way ANOVA with Bonferroni's *post hoc* test, $*p < 0.05$, $**p < 0.01$, $***p < 0.001$ (above bars *versus* control).

GO Ag delivery modifies DC activation of $CD8^+$ T cells

We next examined the ability of DCs cultured with GO–OVA complexes to stimulate $CD8^+$ T cells. OVA alone or adsorbed to sGO or LGO was added to immature BMDCs, which were then co-cultured with CFSE-labelled OT-I $CD8^+$ T cells (Fig. 6A). BMDCs were able to cross-present exogenous OVA Ag *via* MHCI, as measured by induction of OT-I proliferation (Fig. 6B and C). Although sGO–OVA had little influence over the ability of DCs to induce OT-I proliferation compared to OVA alone, LGO–OVA significantly increased this aspect of $CD8^+$ T cell activation (Fig. 6B and C). In contrast, LGO adsorbed to the

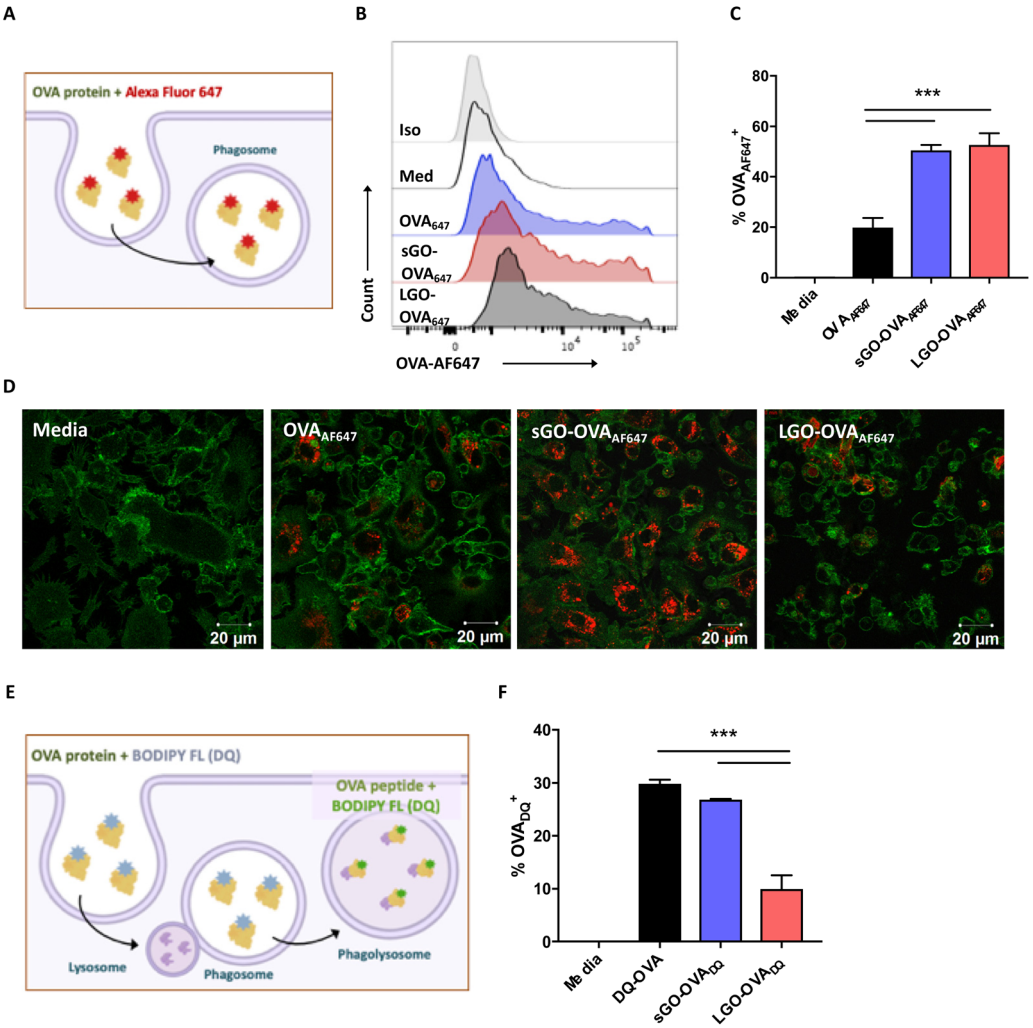

Fig. 3 sGO and LGO enhance DC Ag uptake, while LGO impairs antigen processing. (A) Schematic illustrating the phagocytosis of fluorescently labelled OVA_{AF647} into BMDCs. (B–D) BMDCs were incubated with 10 μg ml^{-1} OVA-AlexaFluor647 or GO–OVA_{AF647} complexes (5 μg : 10 μg) for 30 min. (B and C) Uptake of OVA was quantified by flow cytometry. (D) Uptake of OVA_{AF647} (excitation at 633 nm/emission max at 665 nm, red) was imaged by confocal micros copy, with CellMask Green plasma membrane stain (excitation at 488 nm/emission max at 520 nm, green). Scale bar: 20 μm. (E) Schematic illustrating the processing of OVA in BMDCs. (F) BMDCs were incubated with 10 μg ml^{-1} OVA-DQ or GO–OVA_{DQ} complexes (5 μg : 10 μg) for 30 min, then OVA processing quantified by flow cytometry, with % $OVA_{DQ}{}^{+}$ calculated by subtracting 4 °C values from 37 °C values. (C and F) Data are presented as mean ± STDEV (data is representative of 1 of 3 independent experiments each with 3 intra experimental replicates). Statistical analysis was performed by one-way ANOVA with Bonferroni *post hoc* test, ***$p < 0.001$.

MHCI-restricted peptide OVA_{257} ($OVA_{257–264}$; SIINFEKL) had little effect on DC induction of OVA_{257} specific proliferation, whereas sGO significantly impaired this process (Fig. 6D and E).

In terms of cytokines, the level of IL-2, which is also important for $CD8^{+}$ T cell proliferation,[40] was significantly upregulated in LGO–OVA DC/OT-I co-cultures, compared to DCs exposed to OVA alone or sGO–OVA (Fig. 7A). IFN-γ and granzyme B levels were also dramatically increased in co-cultures containing LGO–OVA, but not sGO–OVA, DCs (Fig. 7A). In comparison, neither sGO nor LGO had a major beneficial or detrimental impact on DC ability to induce OVA peptide-specific cytokine production by OT-I cells, with marginally more effect of LGO than sGO in this regard (Fig. 7B).

The presentation of the MHCI-restricted peptides by either direct loading of DCs with $OVA_{257–264}$, or cross-presentation of peptide derived from processed OVA protein, is a critical signal for effective CTL activation.[41] BMDC expression of SIINFEKL/H-2Kb complexes (pMHC-I) was assessed using an antibody that recognises SIINFEKL bound to H2-Kb of MHCI, following overnight DC culture with OVA protein or OVA_{257} peptide, alone or complexed to GO. DC culture with OVA protein, sGO–OVA or LGO–OVA failed to significantly increased detectable MHCI-restricted SIINFEKL, compared to DCs alone (Fig. S5A and B†). However, sGO adsorption to OVA_{257} peptide resulted in significantly reduced levels of SIINFEKL/H-2Kb complexes, compared to DCs cultured with OVA_{257} alone (Fig. S5C and D†).

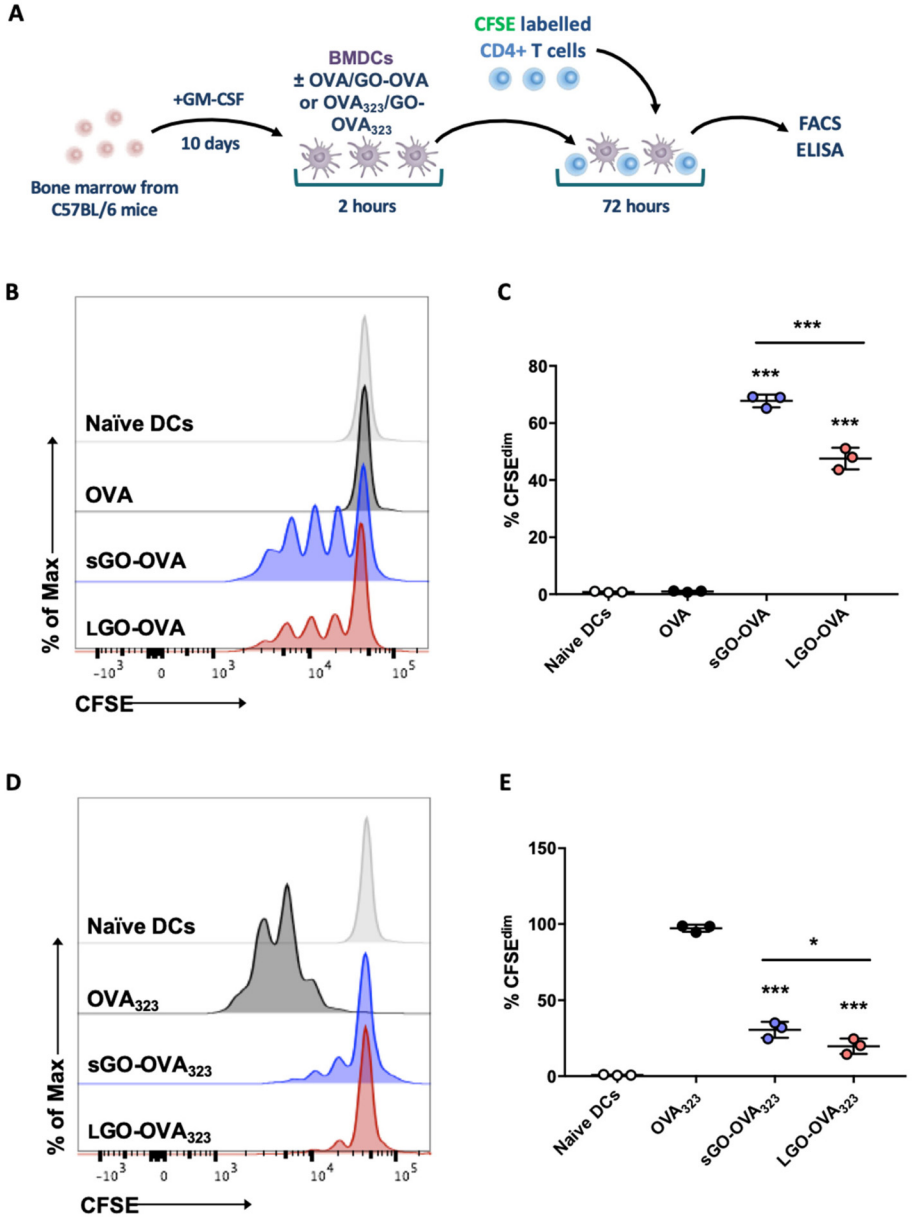

Fig. 4 GO modifies DC induction of proliferation by $CD4^+$ T cells. (A) BMDCs were pulsed for 2 h with 10 μg OVA protein or GO–OVA complexes (5 μg : 10 μg). BMDCs were then washed and co-cultured with CFSE labelled OT-II $CD4^+$ T cells for 72 h. (B and C) Proliferation of OT-II $CD4^+$ T cells was analysed *via* flow cytometry. (B) Representative flow cytometry histogram showing proliferation based on CFSE expression in $CD4^+$ T cells. (C) Proliferation was assessed by CFSE dilution. (A) BMDCs were pulsed for 2 h with 0.05 μg OVA peptide (323–339) or GO–OVA peptide complexes (5 μg : 0.05 μg). (D and E) BMDCs were then co-cultured with CFSE labelled OT-II $CD4^+$ T cells for 72 h. (D) Representative flow cytometry histogram showing proliferation based on CFSE expression in $CD4^+$ T cells. (E) Proliferation was assessed by CFSE dilution. (C and E) Data are presented as mean ± STDEV (data is representative of 1 of 3 independent experiments each with 3 intra experimental replicates). Statistical analysis was performed by one-way ANOVA with Bonferroni's *post hoc* test. ***$p < 0.001$ (above bars *versus* OVA alone control or OVA_{323} alone control).

Together, these data show that LGO can enhance the ability of DCs to process and/or present protein or peptide Ag to activate $CD8^+$ T cells towards a CTL phenotype, while sGO has minimal effect on these events. In comparison, both sGO and LGO can enhance protein Ag specific $CD4^+$ T cell proliferation and cytokine production, but interfere with peptide Ag induction of these outcomes.

GO Ag delivery has minimal effect on DC activation and $CD4^+$ T cell expansion *in vivo*

GO–OVA was administered intravenously to C57BL/6 mice to assess the impact of GO–Ag delivery on DCs *in vivo*. There was a small but significant increase in the percentage and total number of $XCR1^+$ cDC1s 24 h post administration of sGO and

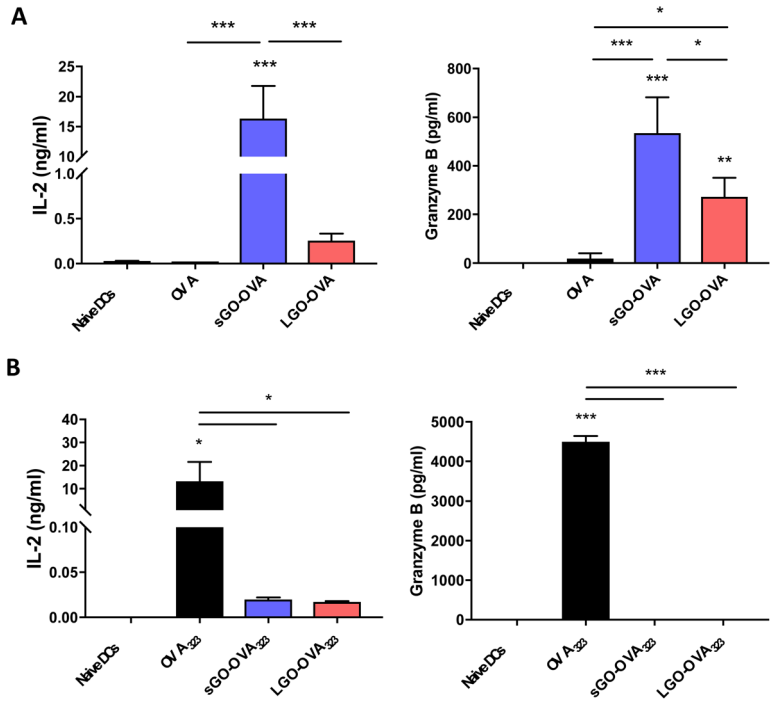

Fig. 5 GO modifies DC induction of cytokine production by $CD4^+$ T cells. (A) BMDCs were pulsed for 2 h with 10 μg OVA protein or GO–OVA complexes (5 μg : 10 μg). BMDCs were then washed and co-cultured with CFSE labelled OT-II $CD4^+$ T cells for 72 h. The levels of IL-2 and granzyme B were assessed in supernatants. (B) BMDCs were pulsed for 2 h with 5 ng OVA peptide (323–339) or GO–OVA peptide complexes (5 μg : 5 ng). BMDCs were then co-cultured with CFSE labelled OT-II $CD4^+$ T cells for 72 h and levels of IL-2 and granzyme B assessed in supernatants. Data are presented as mean ± STDEV (data is representative of 1 of 3 independent experiments each with 3 intra experimental replicates). Statistical analysis was performed by one-way ANOVA with Bonferroni's *post hoc* test. ***$p < 0.001$ (above bars *versus* naïve DCs).

sGO–OVA (Fig. 8A and B). However, no significant change in cDC1 activation was observed, with the intensity of CD80 remained unchanged between groups (Fig. 8C). A similar trend was observed for $CD11b^+$ cDC2s, with the total number of cDC2s significantly increased upon administration of sGO–OVA when compared to all other groups (Fig. 8E), but no change to activation as indicated by intensity of CD80 (Fig. 8F).

To determine whether GO affects surface MHCII-restricted Ag and subsequent T cell activation *in vivo*, the effect of sGO–OVA on antigen specific T cell expansion was assessed. $CD4^+$ T cells isolated from OT-II $Rag1^{-/-}$ × Pep3 were transferred to C57BL/6J mice, prior to immunisation with OVA alone, sGO alone, sGO–OVA or LPS + OVA. Five days post immunisation, spleens were harvested and the level of antigen specific T cell expansion assessed by flow cytometry. Although the relative proportion of $CD45.1^+$ OT-II cells increased upon immunisation with LPS + OVA as expected, no proportional change in OT-II cells was observed upon immunisation with sGO–OVA, when compared to OVA alone (Fig. 8G). This trend was confirmed by quantification of the total number of $CD4^+$ $CD45.1^+$ OT-II cells, where sGO–OVA induced no expansion of OVA specific T cells while LPS + OVA induced a significant expansion of T cells (Fig. 8H), likely due to the significant increase in total number of splenocytes observed with LPS + OVA (Fig. 8I). These data suggest that sGO has minimal ability to activate splenic DC subsets or antigen specific $CD4^+$ T cell expansion *in vivo*.

Discussion

With ever-increasing interest in the potential therapeutic application of GO in disease settings, it is crucial to understand how it affects immune cells, especially those which play a central role in orchestrating adaptive immunity and inflammation. This study aimed to determine the effect of GO of different lateral dimensions on DC maturation and ability to influence $CD4^+$ and $CD8^+$ T cell proliferation and cytokine production. Using murine primary BMDCs and *in vivo* immunisation, we found that GO has little effect on DC viability, and limited impact on DC phenotypic activation or cytokine production. Nevertheless, GO was able to modify DC function, increasing uptake of the model Ag OVA, and modulating their ability to induce Ag-specific $CD4^+$ and $CD8^+$ T cell proliferation and cytokine production *in vitro*.

Understanding whether GO displays toxicity for immune cells was an important first question, central to determining the therapeutic potential of such materials. Consistent with previous reports,[28] we observed negligible cytotoxic effects from exposure of sGO or LGO on BMDC viability, with some effect only evident at high concentrations and most apparent

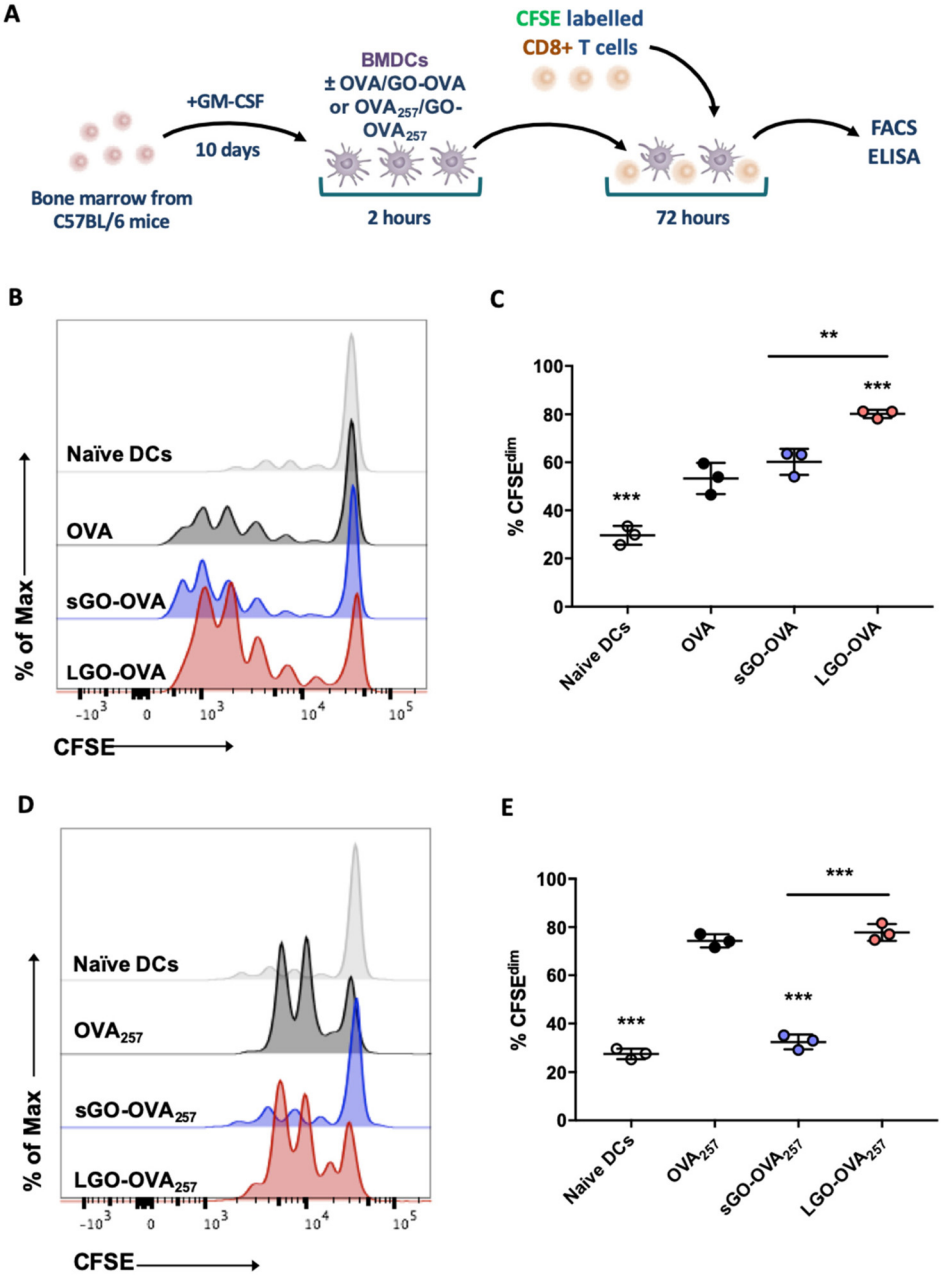

Fig. 6 GO modifies DC induction of proliferation by $CD8^+$ T cells. (A) BMDCs were pulsed for 2 h with 10 μg OVA protein or GO–OVA complexes (5 μg : 10 μg). BMDCs were then washed and co-cultured with CFSE labelled OT-I $CD8^+$ T cells for 72 h. (B and C) Proliferation of OT-I $CD8^+$ T cells was analysed *via* flow cytometry. (B) Representative flow cytometry histogram showing proliferation based on CFSE expression in OT-I $CD8^+$ T cells. (C) Proliferation was assessed by CFSE dilution. (A) BMDCs were pulsed for 2 h with 5 ng OVA peptide (257–264) or GO–OVA peptide complexes (5 μg : 5 ng). BMDCs were then co-cultured with CFSE labelled OT-I $CD8^+$ T cells for 72 h. (D and E) Proliferation of OT-I $CD8^+$ T cells was analysed *via* flow cytometry. (D) Representative flow cytometry histogram showing proliferation based on CFSE expression in $CD8^+$ T cells. (E) Proliferation was assessed by CFSE dilution. (C and E) Data are presented as mean ± STDEV (data is representative of 1 of 3 independent experiments each with 3 intra experimental replicates). Statistical analysis was performed by one-way ANOVA with Bonferroni's *post hoc* test. $^{**}p < 0.01$, $^{***}p < 0.001$ (above bars *versus* OVA alone control or OVA_{257} alone control).

with LGO (Fig. 1A and B). This low-level toxicity, in keeping with similar observations of the same material in macrophages[42] and neutrophils[43] suggests that low concentrations of either s- or LGO minimally impact viability of these important innate immune cells.

In terms of localisation, we were able to visualise sGO in membrane enclosed intracellular vesicles within the cytoplasm (Fig. 1D and F), which are likely part of the endo/lysosomal system. In support of this suggestion, others have performed transmission electron microscopy and confocal microscopy,

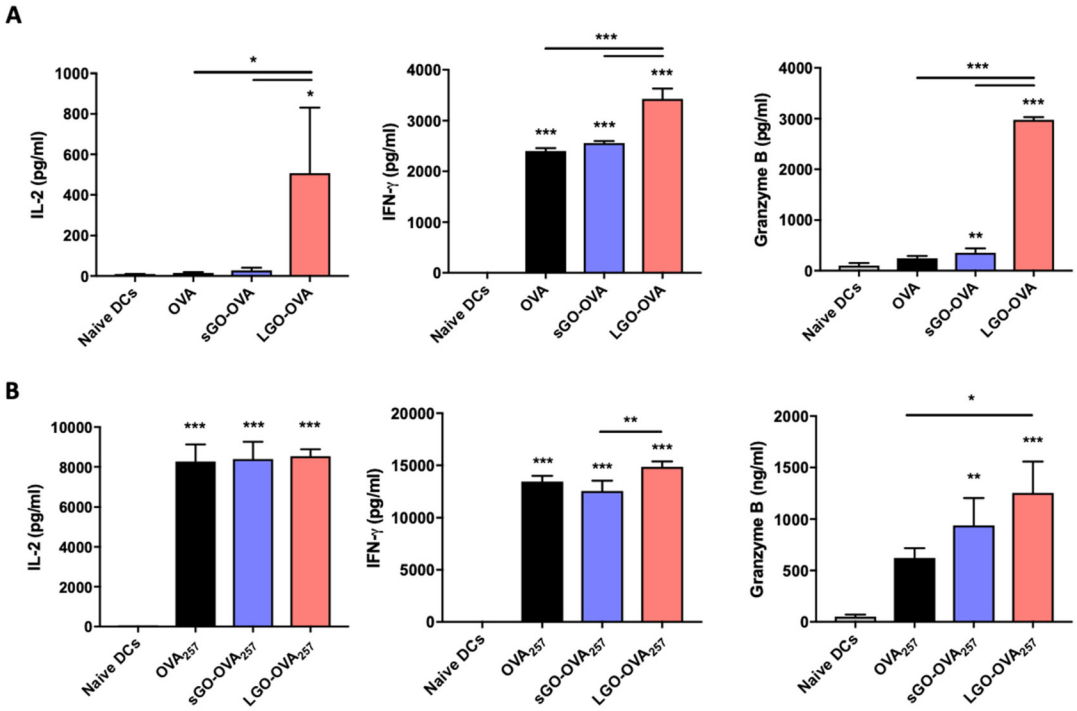

Fig. 7 GO modifies DC induction of cytokine production by $CD8^+$ T cells. (A) BMDCs were pulsed for 2 h with 10 μg OVA protein or GO–OVA complexes (5 μg : 10 μg). BMDCs were then washed and co-cultured with CFSE labelled OT-I $CD8^+$ T cells for 72 h. The levels of IL-2, IFN-γ and granzyme B were assessed in supernatants. (B) BMDCs were pulsed for 2 h with 5 ng OVA peptide (257–264) or GO–OVA peptide complexes (5 μg : 5 ng). BMDCs were then co-cultured with CFSE labelled OT-I $CD8^+$ T cells for 72 h. The levels of IL-2, IFN-γ and granzyme B were assessed in supernatants. Data are presented as mean ± STDEV (data is representative of 1 of 3 independent experiments each with 3 intra experimental replicates). Statistical analysis was performed by one-way ANOVA with Bonferroni's *post hoc* test. ***$p < 0.001$ (above bars *versus* naïve DCs). The levels of IL-4, IL-5, IL-17A, IL-10 and IL-13 were undetectable.

which indicated that GO (similar in size to our sGO) may localise to endosomal/phagosomal compartments within murine BMDCs or human monocyte-derived macrophages.[27,33,44] In contrast to sGO, we observed LGO localisation at the plasma membrane, suggesting it was inefficiently engulfed (Fig. 1F). GO flakes with large lateral dimensions (similar to the LGO in our study) have previously been shown to associate with the plasma membrane of macrophages, with larger GO flakes showing stronger adsorption to the plasma membrane of a murine macrophage-like cell line, whereas smaller GO flakes were readily internalised.[31,45,46]

Formation of a biomolecular corona on the surface of nanomaterials has been shown to modulate their cellular uptake, raising the question as to whether coating GO in Ag or therapeutic drugs may affect such processes.[47] A recent study determined that proteins present in the corona are retained on nanoparticles until they reach the lysosome in murine and human primary DCs, which may be beneficial for MHCII dependent Ag processing and presentation, but may disrupt cross-presentation *via* MHCI.[48] This suggests that Ag processing and presentation may be dependent on the properties of the graphene based material in use, which could help explain why GO of different dimensions displayed differential ability to influence $CD4^+$ or $CD8^+$ T cell proliferation and cytokine production in our work.

During maturation, DCs can upregulate a wide range of surface and costimulatory molecules (including MHCI and II, CD40 and CD80) and secrete a variety of cytokines, the combination of which dictates the character of the subsequent adaptive T cell response.[35,37] We have shown that neither sGO nor LGO induced marked DC maturation, with both failing to trigger dramatic upregulation of MHCI, MHCII, or co-stimulatory molecules, which is in contrast to some previous reports,[27,29] but in agreement with others.[28,30,44,49] These contrasting reports may relate to the purity of the GO used, as DCs are exquisitely sensitive to even trace amounts of contaminants such as endotoxin.[50] As GO also has an innate ability to interfere with the detection wavelength of chromogenic LAL assays, we used a TNF-α expression test (TET) to give a more sensitive, quantitative method for assessing endotoxin contamination in graphene based materials.[51] We would suggest that this kind of sensitive approach to determine endotoxin levels is critical for studies assessing the impact of GO on highly endotoxin-sensitive innate immune cells. In addition to endotoxin, experimental factors that might explain conflicting reports about DC activation by GO include the size and thickness of the materials, their surface chemistry such as the type and amount of oxygen containing surface groups, the concentration added to culture, the type of culture used (primary *vs.* cell line) or the

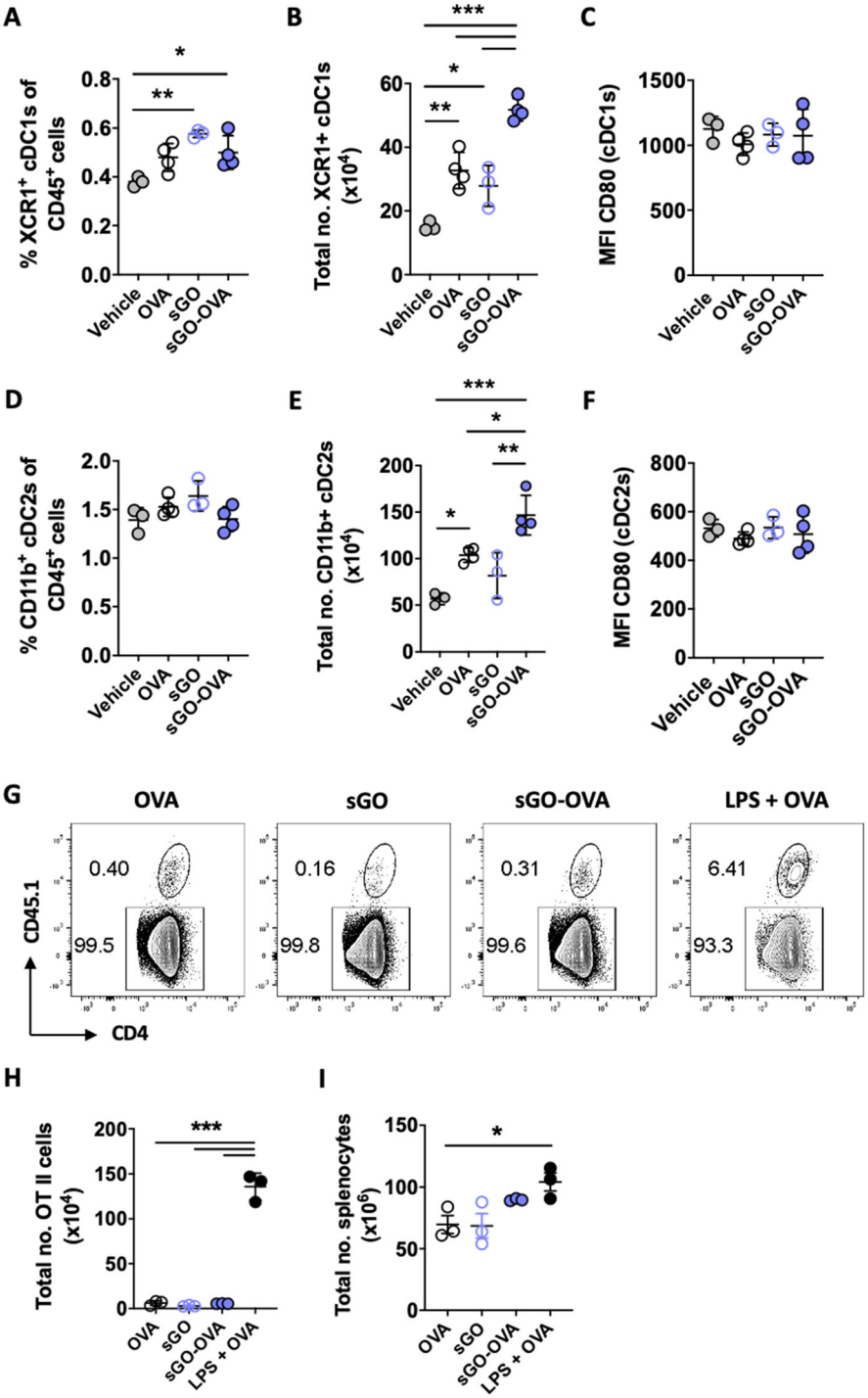

Fig. 8 GO has minimal effect on DC and T cell activation *in vivo*. (A–F) C57BL/6J mice were intravenously administered vehicle, OVA, sGO or sGO–OVA (50 μg GO and 100 μg OVA). After 24 h spleens were harvested and splenic dendritic cell activation assessed by flow cytometry. (A–C) Percentage, total number and CD80 expression of $XCR1^+$ cDC1s. (D–F) Percentage, total number and CD80 expression of $CD11b^+$ cDC2s. (G–I) OVA responsive $CD4^+$ T cells (OT-IIs) were transferred to C57BL/6J mice, the following day mice were intravenously administered OVA, sGO, sGO–OVA or LPS + OVA (250 μg LPS). After 5 days spleens were harvested and OT-II proliferation assessed by flow cytometry. (G) Representative flow cytometry plots of antigen specific and polyclonal $CD4^+$ T cell populations. (H) Total number of antigen specific OT-II cells. (I) Total number of splenocytes. Data are presented as mean ± STDEV (n = 3–4). Statistical analysis was performed by one-way ANOVA with Bonferroni's *post hoc* test. *p < 0.05, **p < 0.01, ***p < 0.001.

length of exposure, all of which could influence viability and/or activation of DCs.

Although we observed little evidence of DC activation by low-endotoxin GO, we did identify a significant increase in CD83 expression by DCs exposed to GO, independent of its lateral dimensions (Fig. 2A, B and S2†). CD83 is a member of the immunoglobulin (Ig) superfamily, blockade of which can inhibit $CD4^+$ T cell responses both *in vitro* and *in vivo*.[52,53] In this way, up-regulation of CD83 expression by both sGO and LGO could help explain why DCs exposed to GO–OVA complexes were able to induce such strong proliferation of $CD4^+$ OT-II cells (Fig. 2A, B and 4B, C). CD83 deficient mice show defective $CD4^+$ T cell development, with $CD8^+$ T cells unaffected,[54] which may relate to why we observed less influence of GO–OVA complexes on $CD8^+$ OT-I cell proliferation. However, it has been suggested that CD83 can provide an important co-stimulatory signal for human $CD8^+$ T cells, and down regulation of CD83 on human monocyte derived DCs results in reduced activation of human $CD8^+$ T cells.[55,56] Thus GO upregulation of CD83 could provide an important costimulatory signal for full activation of Ag-specific $CD4^+$ and/or $CD8^+$ T cells, which may prove useful in cancer and infectious diseases. However, the mechanism by which GO induces DC CD83 expression, independent of lateral dimension and cellular localisation, remains unknown. Further, given this indication that some aspects of DC activation can be initiated by GO, it would be interesting to undertake a broader assessment of DC activation by sGO and LGO using a more objective approach, such as RNA sequencing.

The varying functions of $CD4^+$ T cells are achieved through the differentiation of naïve $CD4^+$ T cells into specialised phenotypes.[57] There are four dominant phenotypes: IFN-γ producing Th1 cells, IL-4 producing Th2 cells, IL-17 producing Th17 cells and regulatory T cells. DCs pulsed with GO–OVA induced significant Ag specific expansion of $CD4^+$ OT-II cells (Fig. 4B and C). Unexpectedly, we identified a $Foxp3^+$ population within proliferating ($CFSE^{dim}$) cells (Fig. S3B†). This transcription factor is often associated with the development of conventional regulatory T cells.[58] This lack of $CD4^+$ T cell effector activation alongside the induction of T_{regs} *in vitro* is most likely a reflection of minimal DC maturation in response to GO.[59–61] We were however unable to detect IL-10, a cytokine commonly associated with these cells,[57] instead identifying their production of granzyme B. Although granzyme B and cytotoxic granules are typically associated with $CD8^+$ CTLs, cytolytic activity of $CD4^+$ T cells during infection has been suggested in recent years.[62] Other studies have also shown that the activity of '$CD4^+$ CTLs' is enhanced when naïve T cells are incubated under neutral (Th0) conditions, similar to those observed with GO–OVA.[63] Additionally, IL-2 signalling is essential for $CD4^+$ CTL induction, as well as Eomes expression, which in turn promotes granzyme B and perforin production.[64] In our experiments, GO–OVA activated DCs significantly induced $CD4^+$ T cell IL-2 production, suggesting that adsorption of Ag to GO may promote a $CD4^+$ CTL cell population that unconventionally expresses the regulatory transcription factor Foxp3. It remains to be determined whether these $CD4^+$ T cells possess cytotoxic or regulatory ability.

Harnessing the ability of DCs to induce Ag-specific $CD8^+$ T cell immunity *via* cross-presentation is required for development of effective vaccines or therapies against many infectious diseases and cancer.[65,66] Our data suggests that LGO may possess the ability to enhance DC ability to induce OVA-specific $CD8^+$ T cell activation (Fig. 6B, C and 7A). This has been seen with treatment of DCs with other nanomaterials – γ-PGA nanoparticles,[67] PLGA nanoparticles,[68] polyethyleneimine nanoparticles[69] or poly(propylene sulphide) nanoparticles[70] promoting OVA cross-presentation in DCs. However, GO has the added benefit of being easily functionalised, with the advantage of biologics adhering to the surface of the material as opposed to being encapsulated, likely allowing more efficient APC uptake. With regards to graphene based materials as Ag carriers, it has been shown that OVA adsorbed to GO can efficiently be internalised by the murine DC cell line DC2.4 and induce OT-I $CD8^+$ T cell proliferation and cytokine secretion.[44] We observed that LGO was beneficial for inducing $CD8^+$ T cell responses, whereas sGO promoted $CD4^+$ T cell responses, likely due to the efficiency of cross presentation being negatively affected by rapid lysosomal degradation of antigens.[71] In contrast, Tkach and colleagues showed that GO suppresses OVA presentation to $CD8^+$ T cells, with GO pre-treatment inhibiting DC activation of OVA-specific B3Z T cells, dependent on DC down regulation of the immunoproteasome subunit LMP7, which is responsible for Ag processing for MHCI presentation.[27] It is possible that pre-treatment with GO prior to Ag exposure may affect DC maturation and MHCI Ag-processing machinery. The effect of GO on Ag cross-presentation remains to be fully understood.

Although all of our work was carried out with pure, low-endotoxin GO, its remarkable adsorbance features may provide a tractable system for modification of DC functionality in a bespoke manner. For example, GO functionalisation with adjuvants such as the TLR agonists CpG-oligodeoxynucleotides and poly(I:C) could further enhance the Th1 and CTL promoting ability of DCs, while use of tolerogenic substances such as vitamin D3 or dexamethasone could favour DC regulatory ability.[72–75] Two recent studies have suggested that GO with adjuvant is able to modulate adaptive immunity more readily. The first of these showed that, when decorated with carnosine and OVA, GO is able to significantly induce an OVA-specific antibody response, as well as increasing splenic populations of polyclonal T cells when compared to GO–OVA alone.[76] The second study focussed on Alum, an aluminium-base adjuvant. When complexed to GO–OVA, Alum was able to induce robust T cell responses and inhibit tumour growth in an E.G7 lymphoma model.[49] These studies suggest that GO may be able to not only boost Ag specific responses, but modulate the adjuvanticity of various biologics. Further work is required to systematically address the full potential of GO functionalisation to provoke immunogenic *vs.* tolerogenic DC ability and its downstream effects on adaptive immunity.

In summary, these novel data provide a foundation for future work to define the impact of GO on other DC types *in vitro*, or following direct administration of GO–Ag complexes *in vivo*. We have identified that low-endotoxin GO, irrespective of its lateral dimensions, induces minimal phenotypic activation of, or cytokine secretion by, DCs. However, GO dimensions influence its uptake by DCs, and differentially affect DC processing and/or presentation of Ag to $CD4^+$ and $CD8^+$ T cells. When complexed with sGO, the model protein Ag OVA could still be effectively processed and presented by DCs to $CD4^+$ OT-II cells, inducing proliferation, Foxp3 expression and granzyme B secretion. In contrast, LGO–OVA complexes were able to promote $CD8^+$ T cell activation and cytokine production. Of note, GO had different effects on DC ability to present peptide Ag to $CD4^+$ *vs.* $CD8^+$ T cells. While $CD8^+$ T cell peptide-specific proliferation and cytokine production were generally only marginally influenced by GO, $CD4^+$ T cell peptide-specific responses were dramatically impaired. This indicates that, while GO enhances DC processing and/or presentation of protein Ag to either $CD4^+$ or $CD8^+$ T cells, it has little impact on presentation of peptides *via* MHCI, and actively interferes with presentation of peptides *via* MHCII. Whether this interference occurs intra- or extra-cellularly remains to be determined. Irrespective, these data will be important to consider for future vaccines or therapies incorporating GO, strongly suggesting that protein, not peptide, Ags will be most effective for $CD4^+$ and $CD8^+$ T cell activation.

Overall, our data show that GO can play a fundamental role in DC activation and ability to influence diverse aspects of T cell effector function, likely dependent on lateral size, concentration, endotoxin contamination and cellular localisation, all of which need to be taken into account when assessing the effect of GO on immune competent cells. Together, these results promote the use of GO for development of novel protein Ag-based vaccines and therapies that could be beneficial for diverse diseases, infections and cancer.

Experimental

Graphene oxide synthesis

LGO, endotoxin-free, for immunology was produced from graphite powder with a modified Hummers' method, in sterile, non-pyrogenic environment, as reported elsewhere, obtaining a brownish aqueous dispersion of GO.[22] All the reagents were purchased from Merck-Sigma Aldrich, UK. Concentration of LGO was estimated by freeze-drying aliquots and weighing the dry powder. sGO was produced from LGO dispersion by 5 minutes treatment in a water bath sonicator (80 W, 45 kHz; VWR, UK). Remaining larger debris flakes were removed by centrifugation at 13 000*g* for 5 minutes.

Endotoxin assessment

Endotoxin were assessed using a TNF-α expression test (TET) as reported previously,[38] enabling selective and sensitive endotoxin detection. In brief the assessment was composed of two steps: (i) cytotoxicity test to determine non-toxic dose of GO for human monocyte-derived macrophages; (ii) ELISA quantification of TNF-α secretion after exposure of human monocyte-derived macrophages at a non-cytotoxic dose of GO.

Ag adsorption to graphene oxide

OVA protein (10 μg; Invivogen), OVA peptides (5 ng; Invivogen), OVA-AF647 (10 μg; Invitrogen) or OVA-DQ (10 μg; Invitrogen) were adsorbed to 5 μg sGO or LGO. GO and Ag were incubated at room temperature for 7 h. Complexes were then centrifuged at 13 000*g* for 30 minutes at 4 °C. Excess Ag in the supernatant was discarded, and the GO complex pellet washed twice with H_2O (endotoxin free, Sigma), and resuspended in 50 μl H_2O (endotoxin free, Sigma) per 5 μg GO. BCA protein assays (Pierce, Thermofisher) were performed as per the manufacturer's protocol in order to generate adsorbance isotherms and assess the amount of protein bound per μg GO.

Animal models

OT-I × Rag-$1^{-/-}$ and OT-II × Rag-$1^{-/-}$ male mice were bred at the Biological Services Facility, University of Manchester in specific-pathogen-free conditions. Male OT-II $Rag1^{-/-}$ × Pep3 mice were bred at the Biological Services Facility, University of Manchester; Pep3 (B6.SJL-$Ptprc^a$ $Pepc^b$/BoyJ) mice which carry the pan leukocyte marker CD45.1 (The Jackson Laboratory, USA) were bred with male OT-II × Rag-$1^{-/-}$ mice. Male and female C57BL/6J mice were purchased from Envigo, UK. All animals used were aged between 6–8 weeks of age. All animals were housed in a 12/12 h light/dark cycle with food and water provided *ad libitum*. All animals were euthanized in accordance with the Animals (Scientific Procedures) Act 1986, and performed under the ethical approval of the Home Office, UK (P44492AC9).

Murine bone marrow derived dendritic cells (BMDCs)

2×10^6 bone marrow cells were cultured in Fisher bacteriological Petri dishes in 10 ml of complete medium (RPMI 1640 supplemented with glutamine, penicillin, streptomycin, 10% heat-inactivated fetal calf serum, and GM-CSF (20 ng ml^{-1}, Peprotech)). At day 3, 6 and 8 media was changed to replenish GM-CSF. Cells were harvested on day 10 and subsequent experiments carried out in complete medium supplemented with GM-CSF (5 ng ml^{-1}).

Dendritic cell stimulations

BMDCs were seeded at 2×10^6 per well of a 24 well plate (1.04×10^6 cells per cm^2). BMDCs were then cultured for 18 h with media, LGO (1–50 μg ml^{-1}), sGO (1–50 μg ml^{-1}), LPS (100 ng ml^{-1}) or GO–Ag complexes.

OVA-AF647 uptake assay. To assess Ag uptake BMDCs were stimulated with sGO–OVA-AF647 for 30 minutes at 37 °C and 4 °C.

DQ-OVA processing assay. To assess Ag processing sGO–DQ-OVA was added to BMDCs for 20 minutes at 37 °C and 4 °C. The positive signal obtained at 4 °C was subtracted from that obtained at 37 °C.

Confocal Raman mapping

BMDCs were grown at 2×10^6 cells per ml on sterile glass coverslips in 6 well culture plates with 5 μg ml^{-1} LGO or sGO. After 18 h slides were washed with PBS and cells fixed with ice-cold methanol. Raman imaging of BMDCs was completed with a DXRi Raman mapping system (Thermo Fisher Scientific, UK). Raman spectroscopy measurements were completed with the following parameters: λ = 633 nm, 0.4 mW, area size = 0.3 mm^2, spatial resolution = 1 μm. Raman shift range for intensity collection = 1000–2000 cm^{-1}. The instrument had an energy resolution of 2.5 cm^{-1}. Raman maps are presented as an overlap between the Raman map highlighting GO location and the bright field view of the cell culture presenting cell shape and locations on the coverslip.

Transmission electron microscopy and electron diffraction

BMDCs were grown at 2×10^6 cells per ml onto sterile ACLAR® fluorinated-chlorinated resin films, in 6 well culture plates. After 24 h incubation, cells were exposed to LGO or sGO at 5 μg ml^{-1}; non exposed cells were included as negative control. After 24 h exposure, cells were washed with PBS and then fixed with 4% paraformaldehyde/5% glutaraldehyde (Merck, Sigma-Aldrich, UK) in 0.2 M HEPES (Merck, Sigma-Aldrich, UK) buffered water for 4 h. Each specimen was washed 3 times with deionized water (5 min each), submitted to a second fixation with ferrocyanide reduced osmium tetroxide (OsO_4) (Agar Scientific, UK) for 2 h, rinsed with deionized water, and dehydrated in a series of ethanol (Thermo Fisher Scientific, UK) grades (30%, 50%, 70%, 90% and 100%) for 15 min at each grade. This was followed by 2 final washes in 100% acetone (Thermo Fisher Scientific, UK) for 15 min each. Specimens were infiltrated with polypropylene TAAB 812 hard resin (TAAB Laboratories Ltd, UK) in acetone at increasing concentrations (25%, 50%, 75% and 100%). Specimens were left in neat resin for 6 h at room temperature. Following this step, specimens were cured at 60 °C for 48 h to allow for resin polymerization. TEM imaging was performed on ultrathin sections (approximately 60–70 nm thickness) obtained using an Ultracut E ultratome (Reichert-Jung, Austria) and a diamond knife (Diatome 45°, Leica, UK), collected onto coatless 200 mesh thin copper 3.05 mm grids (Electron Microscopy Services, UK) and observed under T-12 Biotwin TEM (Techni, Netherlands) equipped with an Orius CCD SC100 camera (GATAN, UK) at 100 keV.

Electron diffraction. Electron diffraction was used as a mean to confirm the crystalline nature of the materials present in cell ultrathin sections. Selected Area Electron Diffraction (SAED) was performed on a Talos 200X (FEI, Eindhoven, NL) operating at 80 keV and using electron dose rates ranging between 45 $e^- A^{-1} s^{-1}$ and 84 $e^- A^{-1} s^{-1}$. TEM images and SAED patterns were acquired using a FEI Ceta CMOS camera on an area of 3.14×10^{-2} μm^2 and 0.5 μm^2 corresponding to the selected area apertures of 10 μm or 40 μm, respectively. An acquisition time of 1 s was used for the collection of TEM images and SAED patterns. However, for the acquisition of SAED patterns with a 10 μm selected area aperture, the acquisition time was set to of 8 s.

Confocal microscopy

BMDCs were plated out at 5×10^5 cells per quadrant in a Cellview cell culture dish (627870; Greiner Bio-One Ltd). Cells were treated with vehicle, sGO or LGO (5 μg ml^{-1}). Cell membranes were then stained with CellMask Green plasma membrane stain (C37608, dilution 1 : 2500, 488/520 nm; Thermo Scientific). Live cell imaging was performed as described previously.[77] Briefly, GO autofluorescence was detected using CLSM Zeiss 880, objective 40× using 594 nm excitation wavelength and 620–690 nm emission wavelengths. Images and videos were subsequently processed using ZEN, the Zeiss microscope software.

In vitro T cell activation

T cell isolation. Spleens and lymph nodes were isolated from OT-I × Rag-$1^{-/-}$ and OT-II × Rag-$1^{-/-}$ mice and homogenised through a 70 μm cell strainer (Fisher Scientific). Red blood cells were then lysed from splenic samples using RBC lysis buffer (Sigma). $CD8^+$ OT I and $CD4^+$ OT II cells were isolated *via* positive selection using $CD8^+$ (Ly-2) and $CD4^+$ (L3T3) Microbeads (Miltenyi Biotec) according to manufacturer's instructions, respectively. Cells were then labelled with CFSE at 37 °C for 10 minutes before being cultured with pre-stimulated BMDCs.

BMDC-T cell stimulation. BMDCs were seeded at a density of 2×10^6 cells per ml (1.04×10^6 cells per cm^2). For OT-II assays BMDCs were pre-stimulated for 2 h with endotoxin free OVA protein (10 μg ml^{-1}) or $OVA_{323–339}$ peptide (5 ng ml^{-1}), alone or adsorbed to sGO or LGO before washing. 50 000 BMDCs were cultures with 100 000 OT-II cells. For OT-I stimulation, BMDCs were prestimulated for 2 h with endotoxin free OVA protein (150 mg ml^{-1}) or were pre-treated or $OVA_{257–264}$ peptide (5 ng ml^{-1}), alone or adsorbed to sGO or LGO before washing. 50 000 BMDCs were incubated with 50 000 T cells and T cell proliferation and activation was assessed after 3 days.

In vivo immunisation

Myeloid activation and antigen presentation. Female C57BL/6J mice, 6–8 weeks of age were subcutaneously immunized with the indicated vaccines at 0 h in the right dorsal back, medial to the inguinal lymph node. 24 h post administration, animals were euthanized and draining inguinal lymph node and spleens harvested for flow cytometric analysis.

In vivo antigen specific functional assays

T cell isolation. Spleens were isolated from OT-II Rag$1^{-/-}$ × Pep3 male mice, homogenised through a 70 μm strainer and incubated in RBC lysis buffer (Lonza) to generate an RBC-free single cell suspension. T cells were isolated using mouse CD8a (Ly-2) MicroBeads (Miltenyi Biotec), according to manufacturer's instructions.

T cell administration. 1×10^6 $CD4^+$ OT-II cells were transferred into male 7-week-old C57BL/6J mice *via* intravenous injection.

Antigen administration. 24 h post transfer of T cells, C57BL/6J were intravenously immunized with the indicated vaccines in the right dorsal back, medial to the inguinal lymph node. 5 days post administration, animals were euthanized and spleens harvested for flow cytometric analysis.

Flow cytometry

All cells were first stained with Zombie UV viability dye (BioLegend) for 15 minutes at room temperature. DC activation, antigen uptake and presentation were characterised using the antibodies listed in ESI Table S1† for 30 minutes in the presence of FcR-Block (2.4G2). T cell proliferation and activation was characterised using the antibodies listed in ESI Table S2.† Intracellular staining was performed with the eBioscience FoxP3 staining kit (Invitrogen). Samples were acquired through the BD LSRFortessa™ flow cytometer (BD Biosciences) using BD FACSDiva software and all analysis was carried out using FlowJo v.10 software (Tree Star). Fluorescence minus one (FMO) control samples were used to validate flow cytometric data.

Greiss reaction

The Greiss reaction was carried out to measure nitric oxide (NO). The reaction solution was made immediately prior to the assay from a 1 : 1 ratio of sulfanilamide (1%; Sigma S9251) and naphthylethylenediamine dihydrochloride (0.1%; Sigma N9125) both in 2.5% phosphoric acid. 50 μl of reaction solution was added to 50 μl of DC supernatant and the resulting colour change was measured at a wavelength of 570 nm and interpolated using a standard curve of $NaNO_2$ serial dilutions.

Cytokine ELISA (enzyme linked immunosorbent assay)

Cytokines (Granzyme B, IFN-γ, IL-2, IL-4, IL-5, IL-6, IL-10, IL-12p40, IL-12p70, IL-13, IL-17A, TNF-α) were quantified using R&D Systems Duoset ELISA kits and BioLegend ELISA standard sets as per the manufacturer's instructions. Briefly, 96 well plates (Thermo-nunc) were coated with primary cytokine-specific antibody and left to incubate at 4 °C overnight. Plates were washed in PBS/0.1% Tween (PBS-T) (Sigma) and blocked with PBS/10% BSA (Sigma) and incubated at room temperature for 60 minutes. Plates were washed again with PBS-T. 50 μl sample supernatant and recombinant protein standards were added in duplicate and the plates were incubated at 4 °C overnight or room temperature for 2 h. Plates were washed with PBST and 50 μl biotinylated antibody was added per well and incubated at room temperature for 2 h. Plates were then washed with PBS-T before addition of horseradish-peroxidase conjugated streptavidin (R&D Systems). Following incubation at room temperature for 30 minutes all plates were washed thoroughly with PBS-T prior to the addition of 50 μl of 1-Step™ Ultra TMB-ELISA Substrate Solution (Thermo Fisher) to each well. The resulting reaction and colour change was stopped with 50 μl H_2SO_4 per well. The final optical density was measured at 450 nm, with correction of a reference wavelength, 570 nm by a spectrophotometer (i-Tecan) and sample concentrations (x) determined *via* interpolation of a 4-parameter logistic (4-PL) standard curve.

Statistical analysis

Statistical analysis was completed in Graph-Pad Prism software. Normal distribution was assessed *via* a D'Agostino–Pearson's test. One-way ANOVAs with Bonferroni's *post hoc* multiple comparisons were performed to compare the means of each group to each other. Statistical significance was determined as $p < 0.05$.

Abbreviations

Ag	Antigen
DCs	Dendritic cells
GO	Graphene oxide
OVA	Ovalbumin

Author contributions

A. S. M. and K. K. were responsible for conceptualisation of the project. H. P., A. M. G., S. V., L. N., O. C., C. B., K. K. and A. S. M. designed and/or performed the experiments. A. M. G. contributed to the characterization of GO. S. V. performed the uptake and processing experiments using confocal microscopy. L. E. C synthesised the graphene material. L. N., O. C. and C. B. performed the Raman and TEM experiments. H. P. and A. S. M wrote the manuscript, with support from K. K., S. V., C. B. and R. S. D. E. P., S. J. H, K. K. and A. S. M provided supervision.

Conflicts of interest

The authors confirm none has any conflict of interest with this work.

Acknowledgements

This work was supported by the Engineering and Physical Sciences Research Council (EPSRC) under the 2D-Health Programme Grant [EP/P00119X/1]. The Bioimaging Facility Systems Microscopy Centre microscopes used in this study were purchased with grants from BBSRC, Wellcome and the University of Manchester Strategic Fund. Special thanks goes to Dave Spiller for his help with the microscopy. Thank you to Dr John Grainger for supplying us with OT-II × Rag-$1^{-/-}$ mice. The authors thank the staff of the Manchester Biological Services Facility for assistance. We would like to acknowledge Mr Alexander Fordham, NanoInflammation Team, Nanomedicine Lab, University of Manchester for running the endotoxin test of the materials. The Nanomedicine Group at

ICN2 is partially supported by the CERCA programme, Generalitat de Catalunya, and the Severo Ochoa Centres of Excellence programme, funded by the Spanish Research Agency (AEI, grant no. SEV-2017-0706).

References

1 L. Planelles, M. C. Thomas, C. Maranon, M. Morell and M. C. Lopez, Differential CD86 and CD40 co-stimulatory molecules and cytokine expression pattern induced by Trypanosoma cruzi in APCs from resistant or susceptible mice, *Clin. Exp. Immunol.*, 2003, **131**(1), 41–47.
2 R. M. Steinman, Lasker Basic Medical Research Award. Dendritic cells: versatile controllers of the immune system, *Nat. Med.*, 2007, **13**(10), 1155–1159.
3 I. Zanoni and F. Granucci, Regulation of antigen uptake, migration, and lifespan of dendritic cell by Toll-like receptors, *J. Mol. Med.*, 2010, **88**(9), 873–880.
4 A. Katsnelson, Kicking off adaptive immunity: the discovery of dendritic cells, *J. Exp. Med.*, 2006, **203**(7), 1622.
5 M. Merad, P. Sathe, J. Helft, J. Miller and A. Mortha, The dendritic cell lineage: ontogeny and function of dendritic cells and their subsets in the steady state and the inflamed setting, *Annu. Rev. Immunol.*, 2013, **31**, 563–604.
6 M. P. Domogalla, P. V. Rostan, V. K. Raker and K. Steinbrink, Tolerance through Education: How Tolerogenic Dendritic Cells Shape Immunity, *Front. Immunol.*, 2017, **8**, 1764.
7 O. Joffre, M. A. Nolte, R. Sporri and C. Reis e Sousa, Inflammatory signals in dendritic cell activation and the induction of adaptive immunity, *Immunol. Rev.*, 2009, **227**(1), 234–247.
8 E. S. Trombetta and I. Mellman, Cell biology of antigen processing in vitro and in vivo, *Annu. Rev. Immunol.*, 2005, **23**, 975–1028.
9 R. M. Steinman, D. Hawiger and M. C. Nussenzweig, Tolerogenic dendritic cells, *Annu. Rev. Immunol.*, 2003, **21**, 685–711.
10 I. Mellman and R. M. Steinman, Dendritic cells: specialized and regulated antigen processing machines, *Cell*, 2001, **106**(3), 255–258.
11 K. Palucka and J. Banchereau, Dendritic-cell-based therapeutic cancer vaccines, *Immunity*, 2013, **39**(1), 38–48.
12 J. E. McElhaney, G. A. Kuchel, X. Zhou, S. L. Swain and L. Haynes, T-Cell Immunity to Influenza in Older Adults: A Pathophysiological Framework for Development of More Effective Vaccines, *Front. Immunol.*, 2016, **7**, 41.
13 C. M. Hilkens, J. D. Isaacs and A. W. Thomson, Development of dendritic cell-based immunotherapy for autoimmunity, *Int. Rev. Immunol.*, 2010, **29**(2), 156–183.
14 C. Horton, K. Shanmugarajah and P. J. Fairchild, Harnessing the properties of dendritic cells in the pursuit of immunological tolerance, *Biomed. J.*, 2017, **40**(2), 80–93.
15 L. Gelao, C. Criscitiello, A. Esposito, M. De Laurentiis, L. Fumagalli, M. A. Locatelli, *et al.*, Dendritic cell-based vaccines: clinical applications in breast cancer, *Immunotherapy*, 2014, **6**(3), 349–360.
16 B. E. Phillips, Y. Garciafigueroa, C. Engman, M. Trucco and N. Giannoukakis, Tolerogenic Dendritic Cells and T-Regulatory Cells at the Clinical Trials Crossroad for the Treatment of Autoimmune Disease; Emphasis on Type 1 Diabetes Therapy, *Front. Immunol.*, 2019, **10**, 148.
17 I. Zubizarreta, G. Florez-Grau, G. Vila, R. Cabezon, C. Espana, M. Andorra, *et al.*, Immune tolerance in multiple sclerosis and neuromyelitis optica with peptide-loaded tolerogenic dendritic cells in a phase 1b trial, *Proc. Natl. Acad. Sci. U. S. A.*, 2019, **116**(17), 8463–8470.
18 A. W. Thomson, A. F. Zahorchak, M. B. Ezzelarab, L. H. Butterfield, F. G. Lakkis and D. M. Metes, Prospective Clinical Testing of Regulatory Dendritic Cells in Organ Transplantation, *Front. Immunol.*, 2016, **7**, 15.
19 K. Vermaelen, Vaccine Strategies to Improve Anti-cancer Cellular Immune Responses, *Front. Immunol.*, 2019, **10**, 8.
20 T. J. Moyer, Y. Kato, W. Abraham, J. Y. H. Chang, D. W. Kulp, N. Watson, *et al.*, Engineered immunogen binding to alum adjuvant enhances humoral immunity, *Nat. Med.*, 2020, **26**(3), 430–440.
21 M. Chakrabarti, R. Kiseleva, A. Vertegel and S. K. Ray, Carbon Nanomaterials for Drug Delivery and Cancer Therapy, *J. Nanosci. Nanotechnol.*, 2015, **15**(8), 5501–5511.
22 J. Jia, Y. Zhang, Y. Xin, C. Jiang, B. Yan and S. Zhai, Interactions Between Nanoparticles and Dendritic Cells: From the Perspective of Cancer Immunotherapy, *Front. Oncol.*, 2018, **8**, 404.
23 H. Shen, L. Zhang, M. Liu and Z. Zhang, Biomedical applications of graphene, *Theranostics*, 2012, **2**(3), 283–294.
24 L. Feng and Z. Liu, Graphene in biomedicine: opportunities and challenges, *Nanomedicine*, 2011, **6**(2), 317–324.
25 D. Bitounis, H. Ali-Boucetta, B. H. Hong, D. H. Min and K. Kostarelos, Prospects and challenges of graphene in biomedical applications, *Adv. Mater.*, 2013, **25**(16), 2258–2268.
26 R. Munoz, D. P. Singh, R. Kumar and A. Matsuda, Graphene Oxide for Drug Delivery and Cancer Therapy, *Nanostructured Polymer Composites for Biomedical Applications*, Elsevier Inc., 2019, pp. 447–488.
27 A. V. Tkach, N. Yanamala, S. Stanley, M. R. Shurin, G. V. Shurin, E. R. Kisin, *et al.*, Graphene oxide, but not fullerenes, targets immunoproteasomes and suppresses antigen presentation by dendritic cells, *Small*, 2013, **9**(9–10), 1686–1690.
28 L. Xu, J. Xiang, Y. Liu, J. Xu, Y. Luo, L. Feng, *et al.*, Functionalized graphene oxide serves as a novel vaccine nano-adjuvant for robust stimulation of cellular immunity, *Nanoscale*, 2016, **8**(6), 3785–3795.
29 X. Zhi, H. Fang, C. Bao, G. Shen, J. Zhang, K. Wang, *et al.*, The immunotoxicity of graphene oxides and the effect of PVP-coating, *Biomaterials*, 2013, **34**(21), 5254–5261.
30 W. Wang, Z. Li, J. Duan, C. Wang, Y. Fang and X. D. Yang, In vitro enhancement of dendritic cell-mediated anti-glioma immune response by graphene oxide, *Nanoscale Res. Lett.*, 2014, **9**(1), 311.

31 J. Ma, R. Liu, X. Wang, Q. Liu, Y. Chen, R. P. Valle, *et al.*, Crucial Role of Lateral Size for Graphene Oxide in Activating Macrophages and Stimulating Pro-inflammatory Responses in Cells and Animals, *ACS Nano*, 2015, **9**(10), 10498–10515.

32 M. Orecchioni, D. A. Jasim, M. Pescatori, R. Manetti, C. Fozza, F. Sgarrella, *et al.*, Molecular and Genomic Impact of Large and Small Lateral Dimension Graphene Oxide Sheets on Human Immune Cells from Healthy Donors, *Adv. Healthc. Mater.*, 2016, **5**(2), 276–287.

33 S. P. Mukherjee, M. Bottini and B. Fadeel, Graphene and the Immune System: A Romance of Many Dimensions, *Front. Immunol.*, 2017, **8**, 673.

34 A. F. Rodrigues, L. Newman, N. Lozano, S. P. Mukherjee, B. Fadeel, C. Bussy, *et al.*, A blueprint for the synthesis and characterisation of thin graphene oxide with controlled lateral dimensions for biomedicine, *2D Mater.*, 2018, **5**(3), 035020.

35 M. Moser and K. M. Murphy, Dendritic cell regulation of TH1-TH2 development, *Nat. Immunol.*, 2000, **1**(3), 199–205.

36 M. Lechmann, S. Berchtold, J. Hauber and A. Steinkasserer, CD83 on dendritic cells: more than just a marker for maturation, *Trends Immunol.*, 2002, **23**(6), 273–275.

37 S. C. Eisenbarth, Dendritic cell subsets in T cell programming: location dictates function, *Nat. Rev. Immunol.*, 2019, **19**(2), 89–103.

38 S. H. Ross and D. A. Cantrell, Signaling and Function of Interleukin-2 in T Lymphocytes, *Annu. Rev. Immunol.*, 2018, **36**, 411–433.

39 S. P. Cullen, M. Brunet and S. J. Martin, Granzymes in cancer and immunity, *Cell Death Differ.*, 2010, **17**(4), 616–623.

40 S. M. Kahan, R. K. Bakshi, R. Luther, L. E. Harrington, R. C. Hendrickson, E. J. Lefkowitz, *et al.*, IL-2 producing and non-producing effector CD8 T cells phenotypically and transcriptionally coalesce to form memory subsets with similar protective properties, *J. Immunol.*, 2017, **198**(1).

41 M. H. Andersen, D. Schrama, P. Thor Straten and J. C. Becker, Cytotoxic T cells, *J. Invest. Dermatol.*, 2006, **126**(1), 32–41.

42 C. Hoyle, J. Rivers-Auty, E. Lemarchand, S. Vranic, E. Wang, M. Buggio, *et al.*, Small, Thin Graphene Oxide Is Anti-inflammatory Activating Nuclear Factor Erythroid 2-Related Factor 2 via Metabolic Reprogramming, *ACS Nano*, 2018, **12**(12), 11949–11962.

43 S. P. Mukherjee, B. Lazzaretto, K. Hultenby, L. Newman, A. F. Rodrigues, N. Lozano, *et al.*, Graphene Oxide Elicits Membrane Lipid Changes and Neutrophil Extracellular Trap Formation, *Chem*, 2018, **4**(2), 334–258.

44 H. Li, K. Fierens, Z. Zhang, N. Vanparijs, M. J. Schuijs, K. Van Steendam, *et al.*, Spontaneous Protein Adsorption on Graphene Oxide Nanosheets Allowing Efficient Intracellular Vaccine Protein Delivery, *ACS Appl. Mater. Interfaces*, 2016, **8**(2), 1147–1155.

45 J. Russier, E. Treossi, A. Scarsi, F. Perrozzi, H. Dumortier, L. Ottaviano, *et al.*, Evidencing the mask effect of graphene oxide: a comparative study on primary human and murine phagocytic cells, *Nanoscale*, 2013, **5**(22), 11234–11247.

46 H. Yue, W. Wei, Z. Yue, B. Wang, N. Luo, Y. Gao, *et al.*, The role of the lateral dimension of graphene oxide in the regulation of cellular responses, *Biomaterials*, 2012, **33**(16), 4013–4021.

47 V. Francia, K. Yang, S. Deville, C. Reker-Smit, I. Nelissen and A. Salvati, Corona Composition Can Affect the Mechanisms Cells Use to Internalize Nanoparticles, *ACS Nano*, 2019, **13**(10), 11107–11121.

48 W. Ma, T. Smith, V. Bogin, Y. Zhang, C. Ozkan, M. Ozkan, *et al.*, Enhanced presentation of MHC class Ia, Ib and class II-restricted peptides encapsulated in biodegradable nanoparticles: a promising strategy for tumor immunotherapy, *J. Transl. Med.*, 2011, **9**, 34.

49 X. Wang, F. Cao, M. Yan, Y. Liu, X. Zhu, H. Sun, *et al.*, Alum-functionalized graphene oxide nanocomplexes for effective anticancer vaccination, *Acta Biomater.*, 2019, **83**, 390–399.

50 H. Schwarz, M. Schmittner, A. Duschl and J. Horejs-Hoeck, Residual endotoxin contaminations in recombinant proteins are sufficient to activate human CD1c$^+$ dendritic cells, *PLoS One*, 2014, **9**(12), e113840.

51 S. P. Mukherjee, N. Lozano, M. Kucki, A. E. Del Rio-Castillo, L. Newman, E. Vazquez, *et al.*, Detection of Endotoxin Contamination of Graphene Based Materials Using the TNF-alpha Expression Test and Guidelines for Endotoxin-Free Graphene Oxide Production, *PLoS One*, 2016, **11**(11), e0166816.

52 Z. Li, X. Ju, P. A. Silveira, E. Abadir, W. H. Hsu, D. N. J. Hart, *et al.*, CD83: Activation Marker for Antigen Presenting Cells and Its Therapeutic Potential, *Front. Immunol.*, 2019, **10**, 1312.

53 A. T. Prechtel and A. Steinkasserer, CD83: an update on functions and prospects of the maturation marker of dendritic cells, *Arch. Dermatol. Res.*, 2007, **299**(2), 59–69.

54 Y. Fujimoto, L. Tu, A. S. Miller, C. Bock, M. Fujimoto, C. Doyle, *et al.*, CD83 expression influences CD4$^+$ T cell development in the thymus, *Cell*, 2002, **108**(6), 755–767.

55 N. Hirano, M. O. Butler, Z. Xia, S. Ansen, M. S. von Bergwelt-Baildon, D. Neuberg, *et al.*, Engagement of CD83 ligand induces prolonged expansion of CD8$^+$ T cells and preferential enrichment for antigen specificity, *Blood*, 2006, **107**(4), 1528–1536.

56 C. Aerts-Toegaert, C. Heirman, S. Tuyaerts, J. Corthals, J. L. Aerts, A. Bonehill, *et al.*, CD83 expression on dendritic cells and T cells: correlation with effective immune responses, *Eur. J. Immunol.*, 2007, **37**(3), 686–695.

57 J. Zhu, H. Yamane and W. E. Paul, Differentiation of effector CD4 T cell populations (*), *Annu. Rev. Immunol.*, 2010, **28**, 445–489.

58 J. D. Fontenot, M. A. Gavin and A. Y. Rudensky, Foxp3 programs the development and function of CD4$^+$CD25$^+$ regulatory T cells, *Nat. Immunol.*, 2003, **4**(4), 330–336.

59 S. Yamazaki, M. Patel, A. Harper, A. Bonito, H. Fukuyama, M. Pack, *et al.*, Effective expansion of alloantigen-specific Foxp3$^+$ CD25$^+$ CD4$^+$ regulatory T cells by dendritic cells during the mixed leukocyte reaction, *Proc. Natl. Acad. Sci. U. S. A.*, 2006, **103**(8), 2758–2763.

60 S. Yamazaki, T. Iyoda, K. Tarbell, K. Olson, K. Velinzon, K. Inaba, *et al.*, Direct expansion of functional CD25$^+$ CD4$^+$ regulatory T cells by antigen-processing dendritic cells, *J. Exp. Med.*, 2003, **198**(2), 235–247.

61 D. Hawiger, K. Inaba, Y. Dorsett, M. Guo, K. Mahnke, M. Rivera, *et al.*, Dendritic cells induce peripheral T cell unresponsiveness under steady state conditions in vivo, *J. Exp. Med.*, 2001, **194**(6), 769–779.

62 J. Loebbermann, H. Thornton, L. Durant, T. Sparwasser, K. E. Webster, J. Sprent, *et al.*, Regulatory T cells expressing granzyme B play a critical role in controlling lung inflammation during acute viral infection, *Mucosal Immunol.*, 2012, **5**(2), 161–172.

63 D. M. Brown, C. Kamperschroer, A. M. Dilzer, D. M. Roberts and S. L. Swain, IL-2 and antigen dose differentially regulate perforin- and FasL-mediated cytolytic activity in antigen specific CD4$^+$ T cells, *Cell. Immunol.*, 2009, **257**(1–2), 69–79.

64 M. E. Pipkin, J. A. Sacks, F. Cruz-Guilloty, M. G. Lichtenheld, M. J. Bevan and A. Rao, Interleukin-2 and inflammation induce distinct transcriptional programs that promote the differentiation of effector cytolytic T cells, *Immunity*, 2010, **32**(1), 79–90.

65 A. Durgeau, Y. Virk, S. Corgnac and F. Mami-Chouaib, Recent Advances in Targeting CD8 T-Cell Immunity for More Effective Cancer Immunotherapy, *Front. Immunol.*, 2018, **9**, 14.

66 S. Li, A. L. Symonds, T. Miao, I. Sanderson and P. Wang, Modulation of antigen-specific T-cells as immune therapy for chronic infectious diseases and cancer, *Front. Immunol.*, 2014, **5**, 293.

67 T. Yoshikawa, N. Okada, A. Oda, K. Matsuo, K. Matsuo, Y. Mukai, *et al.*, Development of amphiphilic gamma-PGA-nanoparticle based tumor vaccine: potential of the nanoparticulate cytosolic protein delivery carrier, *Biochem. Biophys. Res. Commun.*, 2008, **366**(2), 408–413.

68 C. Song, Y. W. Noh and Y. T. Lim, Polymer nanoparticles for cross-presentation of exogenous antigens and enhanced cytotoxic T-lymphocyte immune response, *Int. J. Nanomed.*, 2016, **11**, 3753–3764.

69 J. Chen, Z. Li, H. Huang, Y. Yang, Q. Ding, J. Mai, *et al.*, Improved antigen cross-presentation by polyethyleneimine-based nanoparticles, *Int. J. Nanomed.*, 2011, **6**, 77–84.

70 S. Hirosue, I. C. Kourtis, A. J. van der Vlies, J. A. Hubbell and M. A. Swartz, Antigen delivery to dendritic cells by poly (propylene sulfide) nanoparticles with disulfide conjugated peptides: Cross-presentation and T cell activation, *Vaccine*, 2010, **28**(50), 7897–7906.

71 D. Accapezzato, V. Visco, V. Francavilla, C. Molette, T. Donato, M. Paroli, *et al.*, Chloroquine enhances human CD8$^+$ T cell responses against soluble antigens in vivo, *J. Exp. Med.*, 2005, **202**(6), 817–828.

72 T. G. Kim, C. H. Kim, E. H. Won, S. M. Bae, W. S. Ahn, J. B. Park, *et al.*, CpG-ODN-stimulated dendritic cells act as a potent adjuvant for E7 protein delivery to induce antigen-specific antitumour immunity in a HPV 16 E7-associated animal tumour model, *Immunology*, 2004, **112**(1), 117–125.

73 D. Sui, L. Ma, M. Li, W. Shao, H. Du, K. Li, *et al.*, Mucin 1 and poly I:C activates dendritic cells and effectively eradicates pituitary tumors as a prophylactic vaccine, *Mol. Med. Rep.*, 2016, **13**(4), 3675–3683.

74 A. S. Farias, G. S. Spagnol, P. Bordeaux-Rego, C. O. Oliveira, A. G. Fontana, R. F. de Paula, *et al.*, Vitamin D3 induces IDO$^+$ tolerogenic DCs and enhances Treg, reducing the severity of EAE, *CNS Neurosci. Ther.*, 2013, **19**(4), 269–277.

75 J. H. Lee, C. S. Park, S. Jang, J. W. Kim, S. H. Kim, S. Song, *et al.*, Tolerogenic dendritic cells are efficiently generated using minocycline and dexamethasone, *Sci. Rep.*, 2017, **7**(1), 15087.

76 C. Meng, X. Zhi, C. Li, C. Li, Z. Chen, X. Qiu, *et al.*, Graphene Oxides Decorated with Carnosine as an Adjuvant To Modulate Innate Immune and Improve Adaptive Immunity in Vivo, *ACS Nano*, 2016, **10**(2), 2203–2213.

77 S. Vranic, A. F. Rodrigues, M. Buggio, L. Newman, M. R. H. White, D. G. Spiller, *et al.*, Live Imaging of Label-Free Graphene Oxide Reveals Critical Factors Causing Oxidative-Stress-Mediated Cellular Responses, *ACS Nano*, 2018, **12**(2), 1373–1389.

